DR. ULRICH ECKHARD (Orcid ID : 0000-0001-5863-4514)
PROF. CATHERINE DAWN VAN RAAMSDONK (Orcid ID : 0000-0002-4309-3513)

Article type : Original Article

Manuscript Category: Development & Stem cells (DSC)

Melanocyte development in the mouse tail epidermis requires the Adamts9 metalloproteinase

Grace Tharmarajah[1], Ulrich Eckhard[2], Fagun Jain[1*], Giada Marino[2*], Anna Prudova[2*], Oscar Urtatiz[1*], Helmut Fuchs[3], Martin Hrabe de Angelis[3,4,5], Christopher M. Overall[2,6], and Catherine D. Van Raamsdonk[1]

[1]Department of Medical Genetics,

Life Sciences Institute,

2350 Health Sciences Mall,

University of British Columbia,

Vancouver, BC, V6T 1Z3, Canada.

[2]Centre for Blood Research,

Department of Oral Biological and Medical Sciences,

Faculty of Dentistry,

Life Sciences Institute,

2350 Health Sciences Mall,

University of British Columbia,

Vancouver, British Columbia, V6T 1Z3, Canada.

[3] German Mouse Clinic,

Institute of Experimental Genetics,

Helmholtz Zentrum Munchen,

German Research Centre for Environmental Health,

Ingolstadter Landstrasse 1,

85764 Neuherberg, Germany.

[4]Chair of Experimental Genetics,

School of Life Science,

Weihenstephan Technische Universitat,

Munchen, Alte Akademie 8,

85354 Freising, Germany.

[5]German Center for Diabetes Research (DZD),

Ingolstadter Landstrasse 1,

85764 Neuherberg, Germany.

[6]Department of Biochemistry and Molecular Biology,

Life Sciences Institute,

2350 Health Sciences Mall,

University of British Columbia,

Vancouver, V6T 1Z3, Canada.

*These authors contributed equally to this work and are listed in alphabetical order.

Corresponding author:

Catherine D. Van Raamsdonk, Ph.D.

cvr@mail.ubc.ca

Phone:604-827-4224

Fax:604-822-5348

SUMMARY

The mouse tail has an important role in the study of melanogenesis, because mouse tail skin can be used to model human skin pigmentation. To better understand the development of melanocytes in the mouse tail, we cloned two dominant ENU-generated mutations of the *Adamts9* gene, *Und3* and *Und4*, which cause an unpigmented ring of epidermis in the middle of the tail, but do not alter pigmentation in the rest of the mouse. *Adamts9* encodes a widely expressed zinc metalloprotease with thrombospondin type 1 repeats with few known substrates. Melanocytes are lost in the *Adamts9* mutant tail epidermis at a relatively late stage of development, around E18.5. Studies of our *Adamts9* conditional allele suggest that there is a melanocyte cell autonomous requirement for *Adamts9*. In addition, we used a proteomics approach, TAILS N-terminomics, to identify new Adamts9 candidate substrates in the extracellular matrix of the skin. The tail phenotype of *Adamts9* mutants is strikingly similar to the unpigmented trunk belt in *Adamts20* mutants, which suggests a particular requirement for Adamts family activity at certain positions along the anterior-posterior axis.

SIGNIFICANCE

This work extends our understanding of the shared functional role of the *Adamts9* and *Adamts20* metalloproteinases in late melanocyte development and illustrates the specialization of these two genes in the trunk and the tail.

Keywords: Melanoblast development, Adamts, metalloproteinase, skin pigmentation, tail.

Running title: Mouse tail melanocytes require Adamts9

INTRODUCTION

Due to the high level of conservation in the pigmentary systems of mice and humans, the modeling of skin pigmentation in the mouse has great potential (Fitch et al., 2003; Van Raamsdonk et al., 2004). The epidermis of the mouse tail is organized into rows of scales, with exactly 3 hair follicles and around 100 inter-follicular melanocytes per scale. Although human skin is not organized into scales, the function of melanocytes is conserved between the species; melanocytes are located at the basal layer of the epidermis and transfer melanosomes to surrounding keratinocytes. The underlying dermis is also populated by melanocytes in the mouse tail, although this is not a typical site for melanocytes in humans. We previously found that the inter-follicular epidermal melanocytes of the mouse tail responded to germline mutations in Neurofibromin *(Nf1)*, recapitulating the *cafe au lait* macules and generalized skin hyper-pigmentation of human neurofibromatosis type 1 (Deo et al., 2012; Deo et al., 2013). In addition, expression of the oncogenic version of the heterotrimeric G protein alpha subunit, *GNAQ,* caused dermal melanocytosis in the mouse tail, while sparing the epidermis, analogous to the effects of oncogenic *GNAQ* mutations in humans (Huang et al., 2015; Van Raamsdonk et al., 2009; Van Raamsdonk et al., 2010). These findings support the usefulness of the mouse tail for modeling skin pigmentation disorders.

To better understand the biology of these inter-follicular melanocytes, we searched for mouse mutants with defects in tail skin pigmentation among a large cohort of mice generated during large scale ENU-mutagenesis screening. We noted two mutants (*Undetermined-3* and *Undetermined-4*) that had a very similar and specific phenotype, which consisted of a white ring in the middle of the tail, with normal pigmentation at the tip and base, as well as in the rest of the body. Already present at weaning age, this ring phenotype was

indistinguishable between *Und3* and *Und4* mice, and no other mouse mutant with a similar phenotype has been reported. Thus, we suspected that a novel gene was involved in regulating skin pigmentation in the mouse tail in these two mutants and the identification of this gene would prove interesting.

In this paper, we report that *Adamts9* is mutant in both *Und3* and *Und4* mice. Strikingly, this tail ring phenotype is directly analogous to the "belt" phenotype present in mutants of the closely related *Adamts20* gene (Silver et al., 2008; Somerville et al., 2003). Although an additive affect between *Adamts9* and *Adamts20* has been previously reported in the trunk, no role for either gene was suspected in the tail, which develops later during development and through a different process involving a multipotent mesenchyme called the tailbud (Beck, 2015). Collectively, the ADAMTS protease family is known to cleave the core protein of most proteoglycans, which alters extracellular matrix organization and function and leads to shedding of the O-linked carbohydrate core protein domain from assembled matrix or cell membranes. In doing so, glycosaminoglycan-bound growth factors can also be mobilized, thereby indirectly influencing cell function (Kelwick et al., 2015). In addition to analyzing the *Und3* and *Und4* alleles, which are splice site mutations, we determined when *Adamts9* is required for tail skin pigmentation during development and created a conditional allele to test the cell autonomous effects of *Adamts9* in melanocytes and keratinocytes. Finally, we identified new *in vivo* candidate substrates for Adamts9 in the skin using a proteomics approach, Terminal Amino Isotopic Labeling of Substrates (TAILS).

MATERIALS AND METHODS

Mice

All experiments involving mice were conducted under the approval of the Animal Care Committee at the University of British Columbia. The *Und3* and *Und4* alleles were recovered from a dominant ENU-mutagenesis screen of C3HeB/FeJ mice conducted at the Helmholtz Zentrum München in Germany (Hrabe de Angelis et al., 2000). They were continually maintained on the C3HeB/FeJ genetic background. *EIIa-cre* (*Tg(EIIa-Cre)C5379Lmgd*), *K14-cre (Tg(KRT14-cre)1Amc/J*), and *Mitf-cre (Tg(Mitf-cre)7114Gsb)* transgenic mice were backcrossed to the C3HeB/FeJ background for at least six generations before use (Alizadeh et al., 2008; Dassule et al., 2000; Lakso et al., 1996). *Dct-LacZ* (*Tg(Dct-LacZ)A12Jkn*) and *Rosa26-Tomato* (*Gt(ROSA)26Sortm14(CAG-tdTomato)Hze/J)* mice were on a mixed C3HeB/FeJ;C57Bl/6J background (Mackenzie et al., 1997; Madisen et al., 2009).

Adamts9^{flox} allele

The conditional *Adamts9*^{flox} allele was generated at inGenious Targeting Laboratory (Ronkonkoma, New York, USA). *Adamts9* was subcloned from the C57BL/6 BAC clone, RP23: 363L15, and used to build a construct that was electroporated into BA1 (C57Bl/6 x 129/SvEv hybrid) embryonic stem cells. Correctly targeted cells were microinjected into C57BL/6 blastocysts. Resulting chimeric mice were mated to C57BL/6 FLP mice to remove the Neo cassette and establish germline transmission. The *Adamts9*^{flox} allele was then backcrossed to C3HeB/FeJ for four generations before further use and thereafter maintained on the C3HeB/FeJ background.

Genotyping

DNA was purified from tissue samples using DNeasy columns (Qiagen) and amplified using PCR. The *Adamts9*^{Und3} and *Adamts9*^{Und4} alleles were genotyped by sequencing the amplicons produced by the Und3-35L,5'-GAAACTGGAAAAGCCAGCAG, Und3-35R,5'-GAAGCCGCTAAAGGTGAGTG, Und4-3L,5'-TGTCCTGCAAACATGGAGAA, and Und4-3R,5'-TTTCTGTTGGCTGAGTCGTG. To genotype the *Adamts9*^{flox} allele, we used NEDL1,5'-CAGGGGAGGTTCTTAGCCTAGT and NDEL2,5'-CCAATAAGCTAGCATCATTCTGTTG. Primers MADA3,5'-CCTGTTACCTCTCAGATCGCTCTC and NDEL2 span the deleted region and only can produce a product from the recombined allele. Cre lines were genotyped as previously described (Alizadeh et al., 2008; Dassule et al., 2000; Lakso et al., 1996)

Skin histology

For X-gal staining, tail skin was excised and the tail bones removed. Skin was stained overnight in X-gal solution at room temperature and the next day the dermis and epidermis were separated and photographed with a stereomicroscope. For detection of Tomato positive cells, tail skin was similarly dissected, the dermis and epidermis were separated, and the epidermal sheet was placed on a slide under a cover slip with PBS and scanned using a 3DHistech fluorescent slide scanner. For the TUNEL assay, epidermal sheets were then fixed overnight in 10% formalin at 4°C in the dark and the TUNEL assay was performed the next morning using the TACS® 2 TdT Fluorescein Kit (Trevigen) with the Cytonin option for permeabilization. Sheets were placed in Vectasheild under a coverslip and then scanned for fluorescein and rescanned for Tomato signal simultaneously.

To separate the dermis from the epidermis, tissue samples were incubated in 2M sodium bromide for 5 min at room temperature (for P0 samples) increasing to 2 hours at 37°C (for P42 samples). Forceps were used to separate the epidermal and dermal sheets.

To assess the amount of skin hypo-pigmentation, the average pixel intensity of group photographed epidermal and dermal sheets was calculated using ImageJ software (National Institutes of Health, Bethesda, MD, USA).

For Adamts9 immunohistochemistry, tail skin was fixed in 4% paraformaldehyde for 20 minutes, incubated in a sucrose gradient, and embedded in Tissue-Tek OCT. 10 micron sections were treated with hydrogen peroxide, blocked, and incubated with primary antibody: RP4-Adamts9 diluted 1:35 overnight at 4°C (Triple Point Biologics). The ABC elite kit (Vector) was used for DAB substrate staining. For Mitf/Tomato immunofluorescence, P0 tail skin was fixed in 10% neutral buffered formalin overnight at 4°C, washed and incubated in a sucrose gradient, and embedded in Tissue-Tek OCT. 10 micron sections were washed with PBS, blocked in 1.5% serum for 5 hours, incubated with anti-Mitf antibody (HPA003259, Sigma) overnight at 4°C, washed with PBS, and incubated with 488 donkey anti-rabbit antibody in PBS + 0.3% Triton X-100 and 5% donkey serum for 1 hour at room temperature. Slides were washed again and viewed with a DMI 600B inverted fluorescent microscope.

TAILS proteomics

In brief, soluble and insoluble protein fractions of four biological replicates of mouse skin were blocked by reductive demethylation using isotopically labeled formaldehyde. +/+ (labeled with heavy formaldehyde) and *Adamts9*^{Und4}/+ (labeled with light formaldehyde) proteomes were combined for TAILS analyses (auf dem Keller et al., 2013). After tryptic digestion, internal tryptic peptides were removed from the N-terminome by a high molecular weight polyaldehyde polymer (HPG-ALD; available through flintbox, http://flintbox.com/public/project/1948/) under reductive conditions. The resulting N-terminome was analyzed by LC-MS/MS on a LTQ-Orbitrap Velos as described in Supplementary Methods.

Statistical Analysis

Data was analyzed by students *t* test for statistical significance. Error bars represent the standard error of the mean.

RESULTS

***Und3* and *Und4* cause a white tail ring phenotype**

To identify genes necessary for caudal melanocyte development, we studied *Und3/+* and *Und4/+* mice, which were recovered during a dominant ENU-mutagenesis screen of C3HeB/FeJ mice (Hrabe de Angelis et al., 2000). *Und3/+* and *Und4/+* mice exhibited a ring of unpigmented skin in the middle of the tail, but were pigmented normally in the rest of the body (**Figure 1A-B**). The most frequently affected area of the tail was located three-quarters of the way from the base to the tip (**Figure 1C**). Progeny with tail rings were observed less frequently than expected in our maintenance crosses on the original C3HeB/FeJ genetic background, and following the molecular identification of the mutations (below), the penetrance of any tail hypo-pigmentation phenotype at weaning age was calculated to be 83% and 71% for the *Und3*/+ and *Und4*/+ genotypes, respectively (**Figure 1D**). There is variable expressivity in the amount of tail hypo-pigmentation, with only 66% and 50% of *Und3*/+ and *Und4*/+ mice exhibiting a full tail ring that encircles the dorsum and ventrum. Unlike C57BL/6J mice, which can have white tail tips, the tails of C3HeB/FeJ mice were fully pigmented (Hirobe, 1991). For example, in our study, only 1 out of 65 C3HeB/FeJ mice exhibited any tail hypo-pigmentation. Within the hypo-pigmented areas of the adult *Und3/+* and *Und4/+* tails, the epidermis is affected, but the dermis is pigmented normally (**Figure 1E-F**).

Splice site mutations in *Adamts9* in *Und3* and *Und4* mutants

To identify the mutation responsible for the *Und4* phenotype, we employed an outcross-backcross mapping strategy. We crossed *Und4*/+ females with white tail rings to Cast/EiJ males. The resulting F1 progeny with tail rings were collected and backcrossed to C3HeB/FeJ mice. Ten of the resulting N1 progeny that exhibited tail rings were selected for an initial genome scan using SSLP makers polymorphic between the C3HeB/FeJ and Cast/EiJ alleles. We searched for regions of the genome that were homozygous for the C3HeB/FeJ allele in all of the progeny with tail rings. In this way, linkage was detected on Chromosome 6. Subsequently, 100 additional *Und4* N1 mapping progeny with tail rings were genotyped with a denser array of SSLP markers on

Chromosome 6, resulting in a 1.3 megabase physical interval for the *Und4* mutation, as defined by the minimal region of C3HeB/FeJ homozygosity in all N1 mice with tail rings (**Figure 2A**).

According to the mouse Ensembl genome database (GRCm38), the 1.3 Mb *Und4* physical interval contains 11 predicted or known genes, including *Adamts9*. We sequenced all 40 *Adamts9* exons in *Und3*/+ and *Und4*/+ DNA (according to Ensembl transcript ENSMUST00000113438). Compared to the C3HeB/FeJ genetic background, on which the *Und3* and *Und4* alleles arose, a donor splice site mutation was found in intron 35-36 in *Und3* and in intron 3-4 in *Und4* (**Figure 2B-C**).

The canonical donor splice site in mammals consists of an almost invariant 5'-GT-3' with the next base usually an A or G (Burset et al., 2000). Using a wider context around the splice site, the Human Splicing Finder prediction program assigns strong donor sites a consensus value (CV) of greater than 80 (Desmet et al., 2009). Using this analysis, the donor sites at wildtype exon 35 and exon 3 were calculated to have a CV of 97.66 and 78.88, respectively. These values fell to 70.83 and 73.85 in the *Und3* and *Und4* alleles. In addition, sequencing of RT-PCR products generated from primers flanking the exon 35-36 or exon 3-4 junctions in *Und3*/+ or *Und4*/+ tail skin RNA revealed incorrectly spliced transcripts (**Figure 3A-C**). In the case of *Und4*, the incorrectly spliced transcript could be inferred to come specifically from the *Und4* allele, because it contained a mutant base (T), and not the wildtype base (A), at position 3 of intron 3-4 (**Figure 3C**). This incorrectly spliced transcript could not include the entire intron, because intron 3-4 is greater than 23 kb in length. Splicing must have occurred within intron 3-4 at a cryptic splice site fairly close to the normal exon-intron junction to produce this slightly larger PCR product. Other transcripts may be present in the mutant that would not be detected by this particular assay, such as a longer read into intron 3-4 or exon 3 skipping. All of these mistakes could lead to gibberish being included in the protein as a result of read through into the intron and/or a frameshift of the reading frame upon return to an exon. We conclude that splicing is impaired by the *Und3* and *Und4* mutations.

To determine the effect of homozygosity of the *Und4* mutation, we intercrossed F1 animals. At weaning age, none of the resulting F2 progeny had inherited two copies of *Und4* based upon the identified mapping boundaries (66 animals genotyped; $p=3x10^{-9}$). This indicates that *Und4* is homozygous lethal, which is consistent with previously described loss-of-function mutations in *Adamts9* (Dubail et al., 2014; Silver et al., 2008).

An engineered knockout allele of *Adamts9* also causes a tail ring phenotype

A tail ring phenotype had not been previously reported in *Adamts9* mutant mice. However, previous mutant alleles of *Adamts9* were studied on the C57Bl/6 background, which is subject to spurious tail hypo-pigmentation that would complicate identification of a incompletely penetrant phenotype. To address this, we engineered an *Adamts9* mutant allele and crossed it to the C3HeB/FeJ genetic background. In this allele (hereafter referred to as "*Adamts9*^{flox}"), exons 4, 5, and 6 of *Adamts9* are deleted upon Cre mediated recombination (**Figure 4A-B**). The deletion of these exons is expected to remove amino acids 227 to 390, which includes part of the peptidase M12B domain.

Mice carrying the *Adamts9*^{flox} allele were crossed to a ubiquitously expressed Cre line, *EIIa-cre*, and then the resulting *Adamts9*^{flox}/+; *EIIa-cre*/+ mice were backcrossed to wildtype C3HeB/FeJ mice to produce mice carrying a germline recombined *Adamts9* allele without Cre (hereafter referred to as "*Adamts9*^{KO}/+"). 5 out of 7 *Adamts9*^{KO}/+ mice exhibited tail rings, while all control littermates were normal (**Figure 4C**). Thus, haploinsufficiency of *Adamts9* definitively causes a tail ring phenotype. We next crossed the *Adamts9*^{KO}/+ mice to *Adamts9*^{Und3}/+ mice for a complementation test. No *Adamts9*^{KO}/*Adamts9*^{Und3} progeny were recovered at wean (53 animals genotyped; $p=1x10^{-7}$), further demonstrating loss-of-function of *Adamts9* in the *Und3* allele. Using immunohistochemistry, we detected Adamts9 protein throughout the skin of normal mice (**Figure 4D**). We conclude that haploinsufficiency of *Adamts9* on the C3HeB/FeJ genetic background causes an incompletely penetrant tail ring phenotype.

The *Adamts9* tail ring phenotype initiates at around postnatal day 0

To study how *Adamts9* regulates melanoblast development in the tail, we crossed *Adamts9*^{Und4}/+ to *Dct-LacZ*/+ in timed matings (**Figure 5**). *Dct-LacZ* is expressed in melanoblasts as early as E9 of development (Mackenzie et al., 1997). At E16.5, we found that melanoblasts extended throughout the tail, with a concentration at the tip. There were similar numbers in *Adamts9*^{Und4}/+ and +/+ embryos (**Figure 5A**). However, two days later (E18.5/P0), 67% of wildtype mice (*n*=9) were affected by an area of reduced melanoblast density, while 100% of *Adamts9*^{Und4}/+ mice contained areas with no melanoblasts at all (*n*=3) (**Figure 5B**). By P2, the number of affected wildtype mice had dropped to 18% (*n*=11), compared to 88% of mutant mice (*n*=8). At P8, all wildtype mice were fully populated, yet 66% of *Adamts9*^{Und4}/+ mice continued to exhibit areas completely lacking melanoblasts (*n*=6 and *n*=3, respectively). At each of these time points, LacZ-positive melanoblasts were observed throughout the dermis in both +/+ and *Adamts9*^{Und4}/+ mice, hence the reduction was specifically in the epidermis. We note that *Dct-LacZ* stains some nerves in the tail dermis,

but these can be distinguished from melanoblasts based on cellular morphology. Identical findings were present in *Adamts9*^{Und3}/+ mice (**Figure 5B** and data not shown). Thus, we conclude that the tail ring phenotype arises during the postnatal period around P0, following a relatively normal establishment of melanoblasts throughout the anterior-posterior axis during embryogenesis.

To determine if there was any change to the size of the tail ring after P8, when the phenotype becomes visible because of a lack of melanin production in the ring, we photographed 5 *Adamts9*^{Und4}/+ pups every other day and measured the distance between 5 marks tattoo-inked along each tail. We found that between P8 and P19, the tail grows relatively evenly along its length; however, there was a trend of slightly less growth towards the tip (**Figure 6A**). The boundaries affected by hypo-pigmentation remained stable over this time period in all 5 mice. At P28, the affected epidermis of *Adamts9*^{Und4}/+ ; *Dct-LacZ*/+ mice continued to have no LacZ-positive cells in the scales or hair (**Figure 6B-C**). Some scales at the edges of the affected skin were lightly pigmented and contained less dendritic melanocytes (**Figure 6B**). We noted pigmented scales directly adjacent to unpigmented scales in the boundary region of *Adamts9*^{Und4}/+ mice, which suggests restriction of melanocyte movement within scales.

Assessment of a melanocyte cell autonomous requirement for *Adamts9*

The generation of the conditional *Adamts9* allele (above) allowed us to investigate whether the requirement for *Adamts9* in melanocyte development is cell autonomous. The pigmentation defect in *Adamts9* mutants is confined to the epidermis. The most abundant cell type in the epidermis is the keratinocytes. To make a conditional knockout in keratinocytes, we used *K14-cre* (Dassule et al., 2000). The *Keratin 14* (*K14*) promoter has been particularly useful in targeting the expression of transgenes to the mitotically active basal layer of mouse epidermis, which produces the stratified epithelium (Vasioukhin et al., 1999). To make a tissue specific conditional knockout in melanocytes, we used *Mitf-cre*. *Mitf-cre* is a 185 kb BAC transgene that has cre inserted into the first exon of the melanocyte specific *Microphthalmia* transcript, produced at the M promoter (Alizadeh et al., 2008). It has previously been used to successfully drive pigmentation phenotypes in hair follicle and skin melanocytes (Alizadeh et al., 2008; Deo et al., 2012; Huang et al., 2015; Urtatiz et al., 2018). Both of these Cre lines were kept on the C3HeB/FeJ genetic background.

We crossed *Adamts9*^{flox}/+ mice to *K14-cre*/+ mice and *Adamts9*^{flox}/+ mice to *Mitf-cre*/+ mice. We found that all *K14-cre*/+; *Adamts9*^{flox}/+ mice possessed normally pigmented tails (*n*=6), while one *Mitf-cre*/+;

Adamts9^{flox}/+ mouse exhibited a small tail ring (*n*=9) (**Figure 6D-E**). No tail hypo-pigmentation was observed in mice of the control genotypes from these crosses (*n*=41). We then intercrossed mice to produce *Mitf-cre*/+; *K14-cre*/+; *Adamts9*^{flox}/+ animals, and found that they were pigmented normally (*n*=3). Hence, neither conditional knockout (*K14-cre* or *Mitf-cre*) fully recapitulated the germline knockout phenotype of the *Adamts9*^{flox} allele. To determine whether this could be due to low cre efficiency, we assessed the activity of cre in *K14-cre* and *Mitf-cre* P0 tails using the *Rosa26-floxed stop-Tomato* ("*R26-Tomato*") fluorescent reporter (Madisen et al., 2010). We found that *K14-cre* led to wide spread expression of Tomato in the epidermis (**Figure 6F**). Melanoblasts staining positive for an Mitf antibody did not express Tomato signal (arrows, **Figure 6F**). Therefore, the efficiency of *K14-cre* appears to be very high and K14 and Mitf expression are mutually exclusive, as expected. To determine the efficiency of *Mitf-cre*, we compared tomato signal with Mitf antibody signal in *Mitf-cre/+; R26-Tomato/+* tail epidermis. *Mitf-cre* induced tomato expression in numerous hair follicle melanoblasts that co-expressed Mitf protein (**Figure 6H**). The efficiency of *Mitf-cre* throughout the epidermis was calculated to be 74% (the fraction of Mitf-positive melanoblasts that were also positive for Tomato) (**Figure 6G-H**). The low penetrance of the tail ring phenotype in *Mitf-cre/+; Adamts9*^{flox}/+ mice may be related to the 74% efficiency of *Mitf-cre*, particularly considering that the tail ring phenotype is not fully penetrant even in *Adamts9*^{KO}*/+* mice.

We next examined the Tomato-positive melanoblasts in *Mitf-cre/+; Adamts9*^{flox}/+; *R26-Tomato/+* mutants. These melanoblasts are presumed to have recombined the *Adamts9*^{flox} allele at the same time as the *R26-Tomato* allele and therefore may have a cell autonomous phenotype detectable on the cellular level. *Rosa26* and *Adamts9* are located within 20 Mb of each other on chromosome 6, so we crossed *Mitf-cre/+; R26-Tomato*/+ males to *Adamts9*^{flox}/+ females in timed matings. We collected the resulting litters at P0 and identified the progeny that carried both *Mitf-cre* and *R26-Tomato* by examining a piece of trunk skin for Tomato signal. We produced epidermal sheets from the tails of the Tomato positive mice and generated a composite image of each whole mounted epidermal sheet using a 3DHistech fluorescent slide scanner. We found Tomato-positive melanoblasts with an abnormal morphology in the *Adamts9*^{flox}/+ samples (*n*=5) (**Figure 7B**), that were not present in wildtype controls (*n*=3)(**Figure 7A**). These melanoblasts were undergoing fragmentation indicating cell death (**Figure 7B,** example cells **#**3-5). In the segment from the 8 mm mark to 12 mm mark along the tails of a matched pair of littermates, we determined that 21% of the Tomato-positive melanoblasts in the *Adamts9*^{flox}/+ sample were abnormal (*n*=112 cells in total) (**Figure 7B**), compared to 0.6% in the +/+ sample (*n*=346 cells in total) (**Figure 7A**). There were also Tomato-positive melanoblasts that appeared to be in the process of cell division or to have recently completed it (see **Figure 7C-D** for examples). These were quantified, but no obvious difference was found between the *Adamts9*^{flox}/+

and +/+ samples (6% vs. 7%, respectively.) In addition, we performed the TUNEL assay to detect double stranded breaks in DNA, also in whole mount format. We found 1 to 3 Tomato/TUNEL-double positive melanoblasts in each *Adamts9*^{flox}/+ sample, but none in wildtype controls. These cells were not yet undergoing fragmentation and probably represent an earlier stage in the process of cell death (**Figure 7E**, note cell undergoing fragmentation directly beneath the TUNEL-positive cell). Taken together, this data suggests that there is a cell autonomous requirement for *Adamts9* in melanoblasts located in the tail epidermis and that a deficiency of *Adamts9* contributes to reduced melanoblast survival. This explains the formation of the tail ring following normal colonization of the tail by melanoblasts at E16. Because numerous Tomato-positive melanoblasts are dying within the *Adamts9*^{flox}/+ epidermis at P0, the ring phenotype is not simply a failure of melanoblasts to cross from the dermis into the epidermis.

As part of a separate study, we sorted Tomato-positive melanocytes from epidermis of *Mitf-cre/+; R26-Tomato/+* tails at P14 and P28 for transcriptome analysis (*full analysis in manuscript in preparation*). From within this dataset, we present here a comparison of the relative expression levels of the 19 *Adamts* family members (**Figure 7F**). The most abundantly expressed *Adamts* gene was *Adamts1*, followed by *Adamts20*. At P14, *Adamts9* was the 6th most abundantly expressed *Adamts* gene, but its expression decreased by P28. *Adamts2, 3, 8, 13, 15, 16, 18*, and *19* were not detectable at either time point.

Proteomic analysis of *Und4* tail skin

Substrates for the Adamts family are difficult to identify using biochemical approaches as these proteinases are large multi-domain, heavily disulfide cross-linked, enzymes up to 220 kDa, thus posing challenges for their recombinant expression with all ancillary domains present (Cerda-Costa and Gomis-Ruth, 2014; Kelwick et al., 2015). This has hampered biochemical investigation of Adamts proteases as these domains include substrate binding exosite domains, and thus are integral to proteolytic and extracellular matrix degradative functions. Hence, in the absence of recombinant protease to screen or validate substrates for Adamts9, we used an unbiased N-terminomics approach known as Terminal Amino Isotopic Labeling of Substrates (TAILS) that has been well established to identify protease cleavage sites and substrates *in vivo* (auf dem Keller et al., 2013; Kleifeld et al., 2010; Kleifeld et al., 2011). Thus, we proteomically quantified the relative abundance of neo N-Termini generated at cleavage sites in one week old +/+ versus *Adamts9*^{Und4}/+ tail skin. 1,777 proteins were identified in total in skin from the base of the tail, including dermis and epidermis (false discovery rate FDR ≤ 1%) (**Supplementary Table 1A**; full details of all peptides identified in preTAILS and TAILS analyses are presented in **Supplementary Table 1 A-G**). 68 peptides occurred with greater frequency in +/+ versus

Adamts9^{Und4}/+ samples following TAILS (**Supplementary Table 1F-a**). Of these, 21 were from extracellular matrix and basement membrane proteins, including biglycan and basement membrane specific heparan sulfate core protein (HSPG), which conform to the proteoglycan substrate specificity profile of Adamts proteases (Apte, 2009). In addition, fibronectin, tenascin, fibrilin-1, and periostin were identified with several cleavage sites found. These initial data identifying potential new candidates for Adamts9 cleavage targets requires follow-up in future proteo-genomic and biochemical studies once methods for expression of recombinant Adamts9 can be established.

DISCUSSION

The modeling of the genetics of skin pigmentation in mice has generally lagged behind understanding of coat color because, for many years, mouse geneticists focused on trunk skin, which is unpigmented. While the tail and its scale organization appears to be dissimilar to human skin, the melanocytes there actively produce melanin and distribute it to surrounding keratinocytes. Alterations in pathways corresponding to those implicated in human skin pigmentation disorders and melanoma have also disrupted pigmentation of the mouse tail skin (Deo et al., 2012; Huang et al., 2015; Kohler et al., 2017; Urtatiz et al., 2018). A number of mouse mutations increase tail skin pigmentation without affecting coat color, and among several large scale ENU-mutagenesis screens, now finished, saturation of this phenotype had not yet been reached (Fitch et al., 2003; Hrabe de Angelis et al., 2000; Van Raamsdonk et al., 2004); hence, many skin specific pigmentation genes remain to be identified. *Und3* and *Und4*, studied in this paper, are the first examples of mutants with a specific pattern of tail skin hypo-pigmentation. We found that both of these mutations are splice site alterations within *Adamts9*, which encodes a widely expressed zinc secreted metalloprotease with thrombospondin type 1 repeats.

Because *Und3* and *Und4* affect the development of melanocytes in the tail, it is necessary to consider how tail development differs from the development of the trunk. The caudal end of the vertebrate body, including all of the tail, is created by the tailbud, a multipotent mesenchyme from which all three germ layers are derived (Beck, 2015; Gofflot et al., 1997; Griffith et al., 1992; Shum et al., 2010). In mice, the tailbud is formed from the remnants of the node and the primitive streak at E12.5. The tailbud generates the notochord, secondary neural tube, muscles and vertebrae. The secondary neural tube is formed from tailbud mesenchyme that undergoes a mesenchymal to epithelial transformation, with cells oriented around a central lumen. The lumen gradually grows larger with the accumulation of additional cells into the tube. It is not known whether

melanoblasts in the tail originate from the tailbud or the secondary neural tube or migrate into the tail from the trunk; however, we found that melanoblasts are present throughout the tail by E16.5.

While a tail spotting phenotype had not been noticed previously in *Adamts9* mutant mice, a role for *Adamts9* in melanocyte development in the trunk was already known (Silver et al., 2008). Because *Adamts9* and *Adamts20* shared high sequence homology, an *Adamts9*; *Adamts20* double mutant mouse was made to determine whether the two genes have overlapping functions. Loss of function mutations in *Adamts20* alone cause the recessive *Belted* phenotype in mice, a ring of unpigmented hair extending all the way around the middle of the trunk with normal pigmentation in the rest of the body (Rao et al., 2003). The additional loss of one knockout allele of *Adamts9* in combination with homozygosity of the $Adamts20^{Bt\text{-}9J}$ allele increased the size of the trunk ring by 25% at birth, immediately after which the double mutants died (Silver et al., 2008). This suggested that *Adamts9* plays a role in melanocyte development in the trunk, however, *Adamts9* plays a more important role in the tail, because the loss of only one copy of *Adamts9* affects tail pigmentation, but not trunk pigmentation. Furthermore, mutations of *Adamts20* have been made on a C3H genetic background and no tail spotting has been reported. We conclude that *Adamts9* is specialized for the tail, whereas *Adamts20* is specialized for the trunk. The distinct mechanism of development of the tail from the tailbud provides a plausible explanation for the necessity of this duplication in gene function.

Between E12.5 and E14.5, melanoblasts in the trunk that are migrating from the dorsum finally reach all areas of the ventrum. Silver et al reported that in *Adamts20* homozygous mutants, there were a normal number of melanoblasts in the trunk until E12.5. Melanoblasts were lost first in the ventrum and then in the dorsum between E14.5 and E16.5 (Silver et al., 2008). We found that $Adamts9^{Und}/+$ embryos possessed a normal number of melanoblasts in the tail at E16.5, but developed a significant loss between P0 and P2. Therefore, in both cases, deficiency of *Adamts* genes induces a late loss of melanoblasts. Rao *et al* (Rao et al., 2003) had previously hypothesized a late role for *Adamts20* in the trunk, based in part upon the observation that the unpigmented area on the back was larger than the unpigmented area on the belly in *Adamts20* mutant mice.

It is striking that the *Adamts20* and *Adamts9* mutations primarily affect the middles of two anterior-posterior axes, one in the trunk and one in the tail. Ring or belt phenotypes that eliminate pigmentation all the way around the dorsal-ventral axis are rare. Most coat spotting mutations affect the belly only, which happens to be the last area reached during migration in the trunk (Baxter et al., 2004). The MGI database lists $Dock7^{Mnlt}$,

Kit, *Mitf*$^{Mi\text{-}crc}$, *Aebp2*$^{Gt(Bc0681)Wtsi}$, *Mcoln3*$^{Va\text{-}J}$, and 15 uncharacterized *Rgsc* Riken mutants with an annotated white tail tip phenotype, but no tail rings. The ENU- mutagenesis screen at the Helmholtz Zentrum München produced no other mouse mutants with tail rings and yet got two independent hits in *Adamts9*. These observations are consistent with a late, specific role for the Adamts protease family in melanoblast development and indicate that they are necessary during the period when the anterior-posterior axes of the trunk and tail are elongating. Why they are needed most in the middle of these anterior-posterior axes remains mysterious. It could be that this portion of the axis grows particularly rapidly at some stage or perhaps has a different extracellular matrix composition less favorable for supporting melanoblast survival.

Adamts20 loss was previously found to increase melanoblast apoptosis, coincident with the disappearance of melanoblasts in *Belted* mice (Silver et al., 2008). Similarly, we observed that conditional *Adamts9* haploinsufficiency driven by *Mitf-cre* in melanoblasts resulted in an abnormal morphology consistent with cell death at P0. From these data, we propose that there is a cell autonomous requirement for *Adamts9* in melanoblasts. Importantly, death occurred after the melanoblasts reached the epidermis, further suggesting that melanoblast migration is not affected in *Adamts9* mutants. A cell autonomous requirement would be surprising because Adamts9 protein expression was detected throughout the tail skin and Adamts9 is a secreted protein. One possibility is that the immediate microenvironment around a melanoblast is altered by its secretion of Adamts9. By releasing glycosaminoglycan-bound growth factors anchored in the extracellular matrix that in turn stimulate melanoblast growth and survival by modulating cell behaviour, Adamts9 may do more than just degrade the extracellular matrix. Indeed, the candidate substrates we identified by TAILS proteomics (see Supplementary Information) include 21 new extracellular matrix and basement membrane proteins, such as basement membrane-specific heparan sulfate core protein and biglycan, that conform to the reported proteoglycan substrate specificity profile of Adamts proteases (Apte, 2009). Alternatively, there could be an intracellular role for Adamts9 within melanocytes. An intracellular role for the *Adamts9* homolog, *Gon-1*, in protein trafficking in the endoplasmic reticulum was reported in *C. elegans*, and some of the candidate substrates that we identified by TAILS are expected to be intracellular (Yoshina et al., 2012).

In summary, the work described here highlights the important role of *Adamts9* in regulating melanoblast survival in the epidermis, which is necessary for normal skin pigmentation. *Adamts9* plays a late role in supporting melanocyte development after the initial phase of melanoblast specification and migration to the epidermis are completed.

ACKNOWLEDGEMENTS

We thank Drs. Ian Jackson and Gregory Barsh for generously providing *Dct-LacZ* and *Mitf-cre* mice. This work was funded by operating grants from the Canadian Institutes for Health Research (MOP-136849, MOP-111055) and the German Federal Ministry of Education and Research (Infrafrontier Grant 01KX1012), with Canadian Foundation for Innovation for infrastructure support. Salary support was provided by the Michael Smith Foundation for Health Research, the National Sciences and Engineering Research Council of Canada, UBC Faculty of Graduate Studies, and the UBC Strategic Training Program in Transfusion Science. C.M.O. is supported by a Canada Research Chair in Protease Proteomics and Systems Biology.

COMPETING INTERESTS

No competing interests to declare.

REFERENCES

Alizadeh, A., Fitch, K. R., Niswender, C. M., Mcknight, G. S., and Barsh, G. S. (2008). Melanocyte-lineage expression of Cre recombinase using Mitf regulatory elements. Pigment Cell Melanoma Res *21*, 63-9.

Apte, S. S. (2009). A disintegrin-like and metalloprotease (reprolysin-type) with thrombospondin type 1 motif (ADAMTS) superfamily: functions and mechanisms. J Biol Chem *284*, 31493-7.

Auf Dem Keller, U., Prudova, A., Eckhard, U., Fingleton, B., and Overall, C. M. (2013). Systems-level analysis of proteolytic events in increased vascular permeability and complement activation in skin inflammation. Sci Signal *6*, rs2.

Baxter, L. L., Hou, L., Loftus, S. K., and Pavan, W. J. (2004). Spotlight on spotted mice: a review of white spotting mouse mutants and associated human pigmentation disorders. Pigment Cell Res *17*, 215-24.

Beck, C. W. (2015). Development of the vertebrate tailbud. Wiley Interdiscip Rev Dev Biol *4*, 33-44.

Burset, M., Seledtsov, I. A., and Solovyev, V. V. (2000). Analysis of canonical and non-canonical splice sites in mammalian genomes. Nucleic Acids Res *28*, 4364-75.

Cerda-Costa, N., and Gomis-Ruth, F. X. (2014). Architecture and function of metallopeptidase catalytic domains. Protein Sci *23*, 123-44.

Dassule, H. R., Lewis, P., Bei, M., Maas, R., and Mcmahon, A. P. (2000). Sonic hedgehog regulates growth and morphogenesis of the tooth. Development *127*, 4775-85.

Deo, M., Huang, J. L., Fuchs, H., De Angelis, M. H., and Van Raamsdonk, C. D. (2012). Differential effects of neurofibromin gene dosage on melanocyte development. J Invest Dermatol *133*, 49-58.

Deo, M., Huang, J. L., and Van Raamsdonk, C. D. (2013). Genetic interactions between neurofibromin and endothelin receptor B in mice. PLoS One *8*, e59931.

Desmet, F. O., Hamroun, D., Lalande, M., Collod-Beroud, G., Claustres, M., and Beroud, C. (2009). Human Splicing Finder: an online bioinformatics tool to predict splicing signals. Nucleic Acids Res *37*, e67.

Dubail, J., Aramaki-Hattori, N., Bader, H. L., Nelson, C. M., Katebi, N., Matuska, B., Olsen, B. R., and Apte, S. S. (2014). A new Adamts9 conditional mouse allele identifies its non-redundant role in interdigital web regression. Genesis *52*, 702-12.

Fitch, K. R., Mcgowan, K. A., Van Raamsdonk, C. D., Fuchs, H., Lee, D., Puech, A., Herault, Y., Threadgill, D. W., Hrabe De Angelis, M., and Barsh, G. S. (2003). Genetics of dark skin in mice. Genes Dev *17*, 214-28.

Gofflot, F., Hall, M., and Morriss-Kay, G. M. (1997). Genetic patterning of the developing mouse tail at the time of posterior neuropore closure. Dev Dyn *210*, 431-45.

Griffith, C. M., Wiley, M. J., and Sanders, E. J. (1992). The vertebrate tail bud: three germ layers from one tissue. Anat Embryol (Berl) *185*, 101-13.

Hirobe, T. (1991). Developmental interactions in the pigmentary system of the tip of the mouse tail: effects of coat-color genes on the expression of a tail-spotting gene. J Exp Zool *258*, 353-8.

Hrabe De Angelis, M. H., Flaswinkel, H., Fuchs, H., Rathkolb, B., Soewarto, D., Marschall, S., Heffner, S., Pargent, W., Wuensch, K., Jung, M., et al. (2000). Genome-wide, large-scale production of mutant mice by ENU mutagenesis. Nat Genet *25*, 444-7.

Huang, J. L., Urtatiz, O., and Van Raamsdonk, C. D. (2015). Oncogenic G Protein GNAQ Induces Uveal Melanoma and Intravasation in Mice. Cancer Res *75*, 3384-97.

Kelwick, R., Desanlis, I., Wheeler, G. N., and Edwards, D. R. (2015). The ADAMTS (A Disintegrin and Metalloproteinase with Thrombospondin motifs) family. Genome Biol *16*, 113.

Kleifeld, O., Doucet, A., Auf Dem Keller, U., Prudova, A., Schilling, O., Kainthan, R. K., Starr, A. E., Foster, L. J., Kizhakkedathu, J. N., and Overall, C. M. (2010). Isotopic labeling of terminal amines in complex samples identifies protein N-termini and protease cleavage products. Nat Biotechnol *28*, 281-8.

Kleifeld, O., Doucet, A., Prudova, A., Auf Dem Keller, U., Gioia, M., Kizhakkedathu, J. N., and Overall, C. M. (2011). Identifying and quantifying proteolytic events and the natural N terminome by terminal amine isotopic labeling of substrates. Nat Protoc *6*, 1578-611.

Kohler, C., Nittner, D., Rambow, F., Radaelli, E., Stanchi, F., Vandamme, N., Baggiolini, A., Sommer, L., Berx, G., Van Den Oord, J. J., et al. (2017). Mouse Cutaneous Melanoma Induced by Mutant BRaf Arises from Expansion and Dedifferentiation of Mature Pigmented Melanocytes. Cell Stem Cell *21*, 679-693 e6.

Lakso, M., Pichel, J. G., Gorman, J. R., Sauer, B., Okamoto, Y., Lee, E., Alt, F. W., and Westphal, H. (1996). Efficient in vivo manipulation of mouse genomic sequences at the zygote stage. Proc Natl Acad Sci U S A *93*, 5860-5.

Mackenzie, M. A., Jordan, S. A., Budd, P. S., and Jackson, I. J. (1997). Activation of the receptor tyrosine kinase Kit is required for the proliferation of melanoblasts in the mouse embryo. Dev Biol *192*, 99-107.

Madisen, L., Zwingman, T. A., Sunkin, S. M., Oh, S. W., Zariwala, H. A., Gu, H., Ng, L. L., Palmiter, R. D., Hawrylycz, M. J., Jones, A. R., et al. (2009). A robust and high-throughput Cre reporting and characterization system for the whole mouse brain. Nat Neurosci *13*, 133-40.

Madisen, L., Zwingman, T. A., Sunkin, S. M., Oh, S. W., Zariwala, H. A., Gu, H., Ng, L. L., Palmiter, R. D., Hawrylycz, M. J., Jones, A. R., et al. (2010). A robust and high-throughput Cre reporting and characterization system for the whole mouse brain. Nat Neurosci *13*, 133-40.

Rao, C., Foernzler, D., Loftus, S. K., Liu, S., Mcpherson, J. D., Jungers, K. A., Apte, S. S., Pavan, W. J., and Beier, D. R. (2003). A defect in a novel ADAMTS family member is the cause of the belted white-spotting mutation. Development *130*, 4665-72.

Shum, A. S., Tang, L. S., Copp, A. J., and Roelink, H. (2010). Lack of motor neuron differentiation is an intrinsic property of the mouse secondary neural tube. Dev Dyn *239*, 3192-203.

Silver, D. L., Hou, L., Somerville, R., Young, M. E., Apte, S. S., and Pavan, W. J. (2008). The secreted metalloprotease ADAMTS20 is required for melanoblast survival. PLoS Genet *4*, e1000003.

Somerville, R. P., Longpre, J. M., Jungers, K. A., Engle, J. M., Ross, M., Evanko, S., Wight, T. N., Leduc, R., and Apte, S. S. (2003). Characterization of ADAMTS-9 and ADAMTS-20 as a distinct ADAMTS subfamily related to Caenorhabditis elegans GON-1. J Biol Chem *278*, 9503-13.

Urtatiz, O., Samani, A. M. V., Kopp, J. L., and Van Raamsdonk, C. D. (2018). Rapid melanoma induction in mice expressing oncogenic Braf(V600E) using Mitf-cre. Pigment Cell Melanoma Res.

Van Raamsdonk, C. D., Bezrookove, V., Green, G., Bauer, J., Gaugler, L., O'brien, J. M., Simpson, E. M., Barsh, G. S., and Bastian, B. C. (2009). Frequent somatic mutations of GNAQ in uveal melanoma and blue naevi. Nature *457*, 599-602.

Van Raamsdonk, C. D., Fitch, K. R., Fuchs, H., De Angelis, M. H., and Barsh, G. S. (2004). Effects of G-protein mutations on skin color. Nat Genet *36*, 961-8.

Van Raamsdonk, C. D., Griewank, K. G., Crosby, M. B., Garrido, M. C., Vemula, S., Wiesner, T., Obenauf, A. C., Wackernagel, W., Green, G., Bouvier, N., et al. (2010). Mutations in GNA11 in uveal melanoma. N Engl J Med *363*, 2191-9.

Vasioukhin, V., Degenstein, L., Wise, B., and Fuchs, E. (1999). The magical touch: genome targeting in epidermal stem cells induced by tamoxifen application to mouse skin. Proc Natl Acad Sci U S A *96***,** 8551-6.

Yoshina, S., Sakaki, K., Yonezumi-Hayashi, A., Gengyo-Ando, K., Inoue, H., Iino, Y., and Mitani, S. (2012). Identification of a novel ADAMTS9/GON-1 function for protein transport from the ER to the Golgi. Mol Biol Cell *23***,** 1728-41.

FIGURE LEGENDS

Figure 1. **White tail ring phenotype in *Und3* and *Und4***

A-B) *Und3*/+ (A) and *Und4*/+ (B) four week old mice. The first mouse in each group of mutants exhibits a mild white patch phenotype; the rest are fully ringed. **C**) Graph showing the affected portion of the tail in *Und3*/+ and *Und4*/+ mice. **D**) Percent of *Und3/+* and *Und4/+* mice with normal pigmentation, a mild white patch phenotype, or a full tail ring on the C3HeB/FeJ background. **E**) Epidermal (top) and dermal (bottom) sheets of mice from affected tail region. The epidermal and dermal sheets are from the same piece of tail and include the border between affected and unaffected epidermis. **F**) Quantification of the average relative pixel intensity of group photographed samples. Skin was sampled from within the hypo-pigmented area.

Figure 2. Splice site mutations in *Adamts9* in *Und3* and *Und4*

A) A map of the physical interval of *Und4* on chromosome 6, according to the Ensembl genome database GRCm38. The recombination fractions are shown below each marker. **B-C**) Base substitutions found in *Und3*/+ (B) and *Und4*/+ (C) genomic DNA, compared to C3HeB/FeJ.

Figure 3. Intron retention in *Adamts9*^{Und} transcripts

A) Schematic showing experimental design for RT-PCR. **B**) Additional bands (stars) result from RT-PCR using RNA from *Und3*/+ and *Und4*/+ neonatal mouse tail skin. **C**) Sequencing traces from *Und3*/+ and *Und4*/+ RT-PCR products in B. The double peaks correspond to the intronic sequence overlaid on the sequence of the next exon.

Figure 4. Conditional allele of *Adamts9*

A) The protein structure of Adamts9, amino acid number shown at top. The locations of the *Und* affected exon junctions are indicated by stars. The *Adamts9* ^{flox} allele targets amino acids 227 to 390. **B)** Creation of the

Adamts9 floxed allele. A, ApaI; X, XbaI; triangles, loxP. **C)** *Adamts9*^{KO}*/+* mice exhibit tail rings, while controls are pigmented normally. **D)** Immunohistochemistry against the Adamts9 propeptide in neonatal mouse tail skin.

Figure 5. Melanoblast deficiency in *Adamts9*^{Und} mutants

A) X-gal stained whole mount *Dct-LacZ*/+ E16.5 tails, +/+ (left) and *Und4*/+ (right). **B**) X-gal stained epidermal (left column) and dermal (right column) sheets from the same representative tails at P0 and P2. At P0, the representative +/+ epidermis exhibits an area of decreased melanoblast density that overlaps the area completely lacking melanoblasts in the representative *Und4*/+ mutant (circled with dashed line). At P2, the representative +/+ epidermis is uniformly populated, while the *Und4*/+ and *Und3*/+ mutants exhibit one or more areas devoid of melanoblasts. The dermis of wildtype and mutants (shown to the right of each epidermis) contains LacZ-positive cells throughout. Nerves in the dermis are also LacZ-positive.

Figure 6. Conditional haploinsufficiency of *Adamts9* in melanocytes or keratinocytes

A) Percent growth of six segments along the tail between P10 and P19, averaged from 5 *Und4*/+ pups. **B**) X-gal stained whole mount *Dct-LacZ*/+; *Und4*/+ P28 epidermal sheets, from the base of the tail (position 1) and from the area around the boundary between the affected and unaffected skin (positions 2 and 3). Arrows indicate LacZ-positive melanocytes. **C**) X-gal stained hairs plucked from the pigmented (left) and unpigmented (right) areas of a *Und4*/+ tail. LacZ-positive melanocytes are present in the pigmented hair bulb (black arrow). **D-E)** Tails from the progeny of *Adamts9*^{flox}*/+* mice crossed to either *K14-cre/+* mice (D) or *Mitf-cre/+* mice (E). Open arrowhead in E indicates a small tail ring in one out of nine *Mitf-cre/+*; *Adamts9*^{flox}/+ mice produced. Mice are 4 weeks of age. **F**) Anti-Mitf antibody staining (green) in PO *K14-cre/+; R26-Tomato/+* tail skin. Tomato signal is shown in red. Arrows indicate Mitf-positive, Tomato-negative cells. **G)** Quantification of cells in *Mitf-cre/+; R26-Tomato/+* tail skin that were either positive for the Mitf antibody signal only, positive for Tomato signal only, or positive for both signals. 74% of Mitf ab positive cells also expressed Tomato, while 84% of Tomato positive cells were also positive for Mitf protein. That not all Tomato positive cells were positive for Mitf ab could be due to a failure of antibody staining or to cells that currently express low levels of Mitf protein. **H)** Anti-Mitf antibody staining in PO *Mitf-cre/+; R26-Tomato/+* tail skin. Double positive Mitf/Tomato melanoblasts were located in characteristic locations in hair follicles ("hf" - traced with dashed line). Scale bars represent 40 μm.

Figure 7. Cell death in *Adamts9* haploinsufficient melanocytes at P0

A-B) Tomato signal (red) in tail epidermal sheets from P0 *Mitf-cre*/+; +/+; *R26-Tomato*/+ (A) or *Mitf-cre*/+; *Adamts9*^{flox}/+; *R26-Tomato*/+ (B) littermates. Example melanoblasts 1 and 2 are a normal spherical shape, while example melanoblasts 3-5 are undergoing fragmentation. Scale bars represent 50 μm (boxed fields) or 20 μm (individual cells). **C-D**) Representative Tomato positive proliferative melanoblasts. Left, melanoblast in the process of division along the midline; Right, melanoblasts within 3 μm of each other, presumed to have recently divided. Scale bar represents 20 μm. **E**) A TUNEL positive (green) melanoblast is indicated by an arrow in an *Mitf-cre*/+; *Adamts9*^{flox}/+; *R26-Tomato*/+ whole mount epidermal sheet. Tomato signal (red) is weaker in the TUNEL-positive melanoblast than in the normal shaped melanoblast located just above it. A melanoblast undergoing fragmentation is below. Scale bar represents 20 μm. **F)** Relative expression of *Adamts* family members in FACS sorted *Mitf-cre*/+; *R26-Tomato*/+ P14 and P28 epidermal tail melanocytes analyzed by RNAseq.

Tharmarajah Figure 1

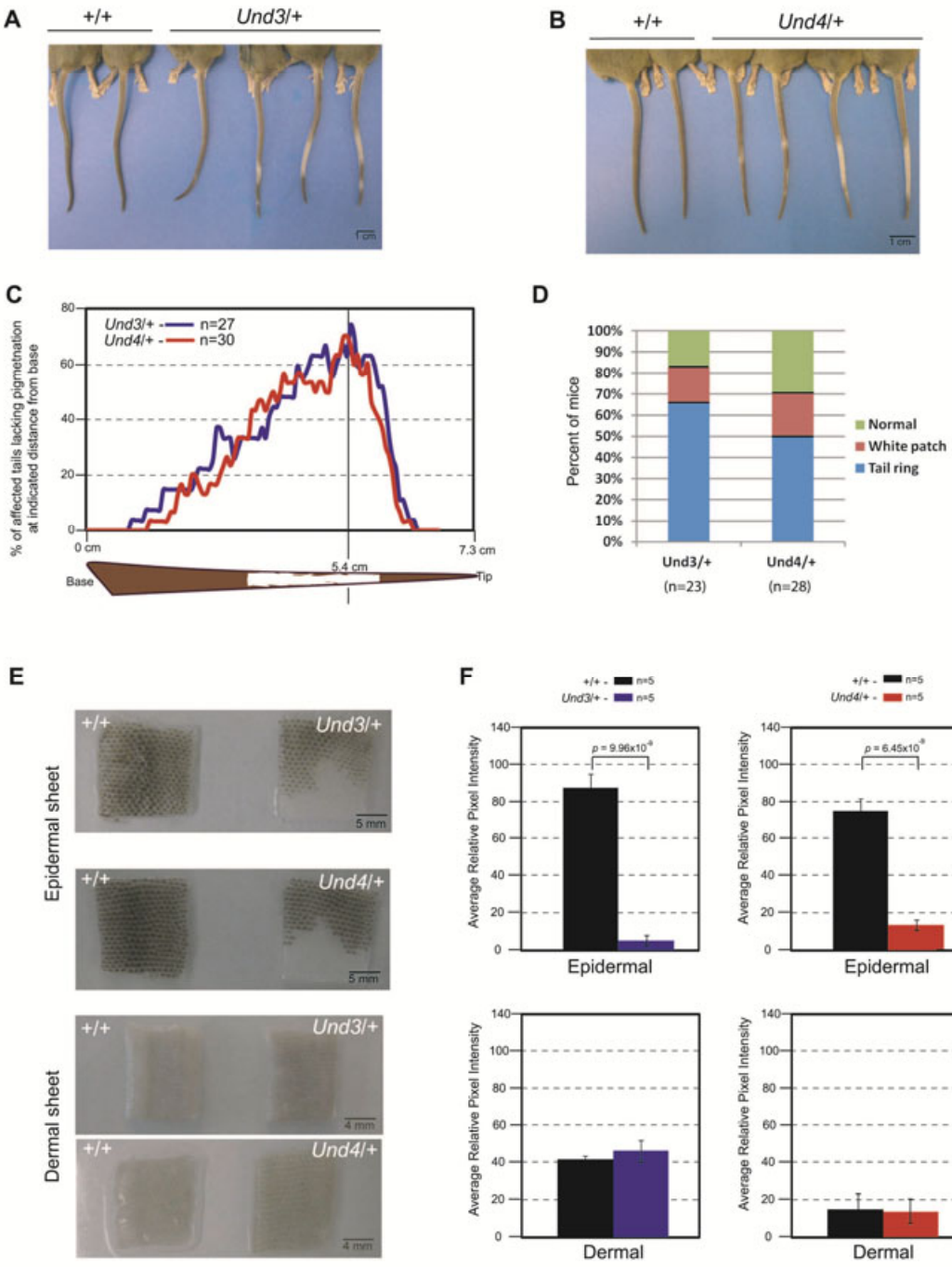

Tharmarajah Figure 2

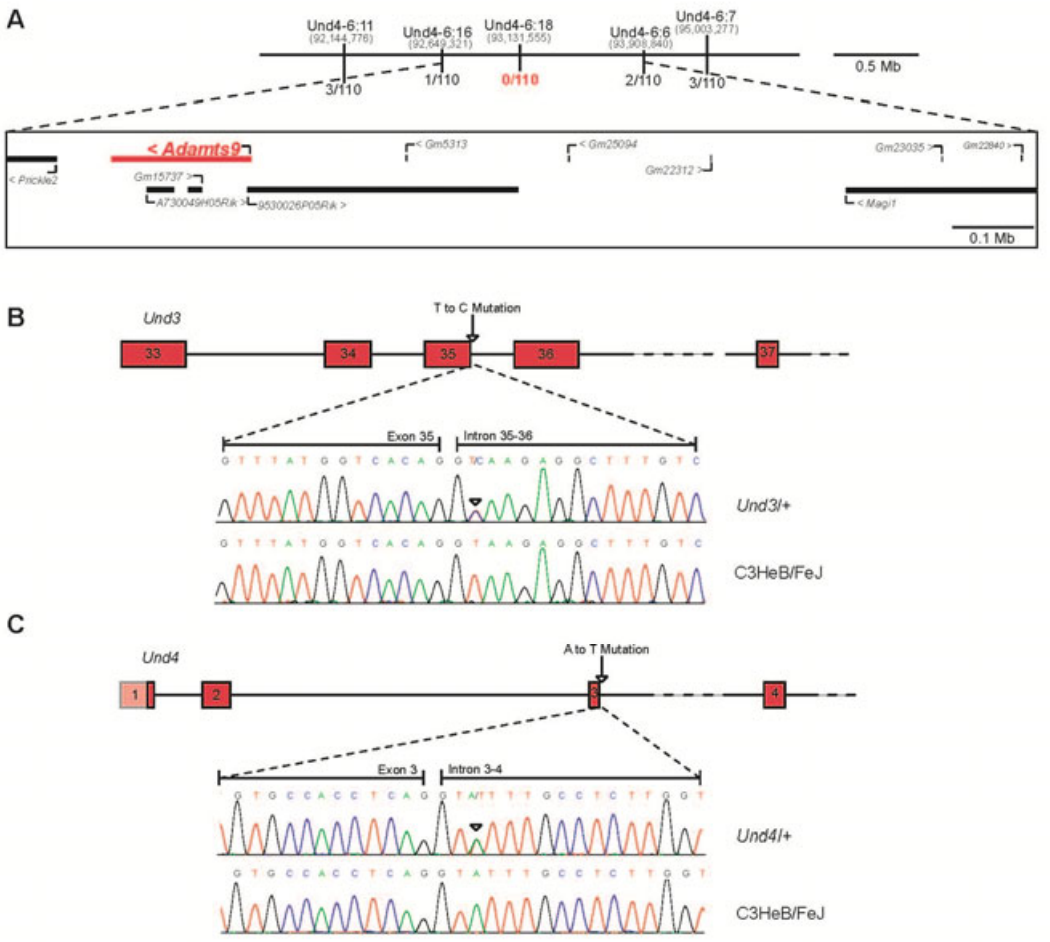

Tharmarajah Figure 3

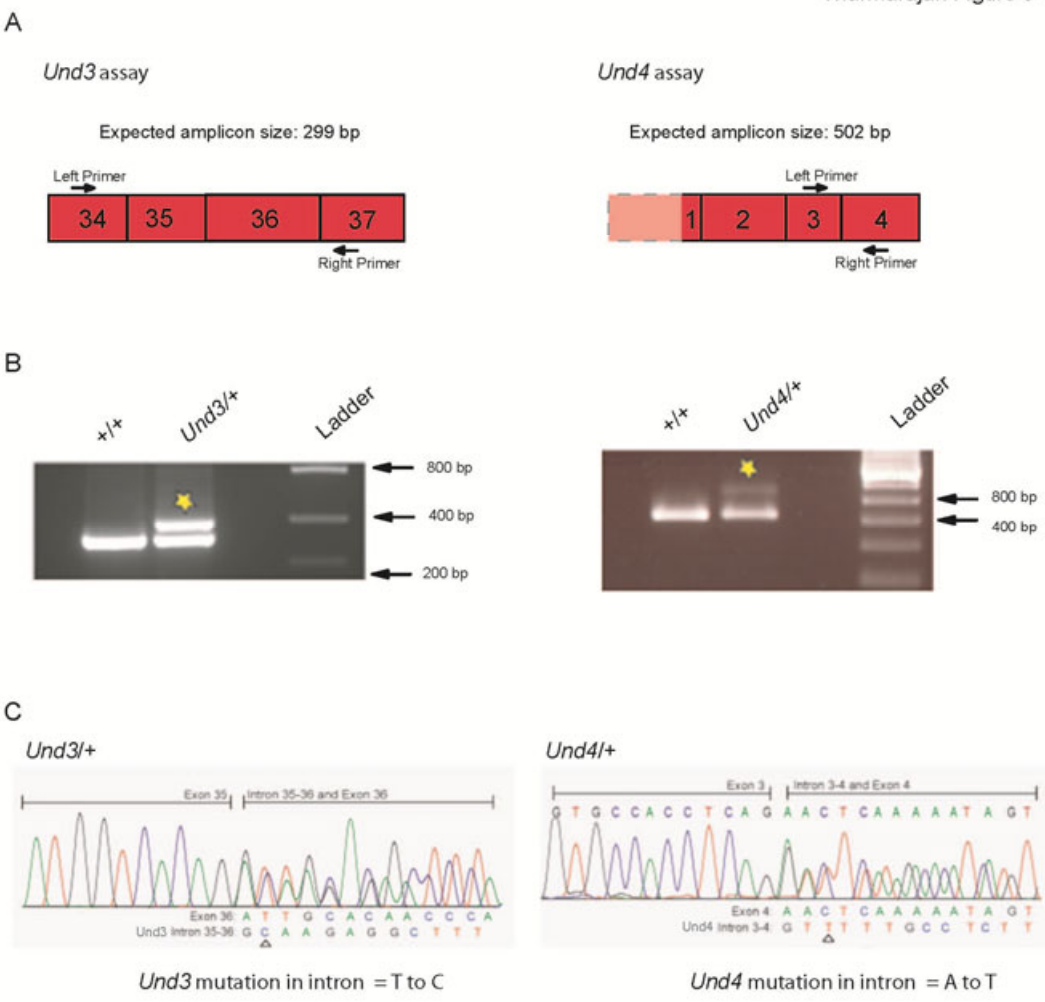

Und3 mutation in intron = T to C

Und4 mutation in intron = A to T

Tharmarajah Figure 4

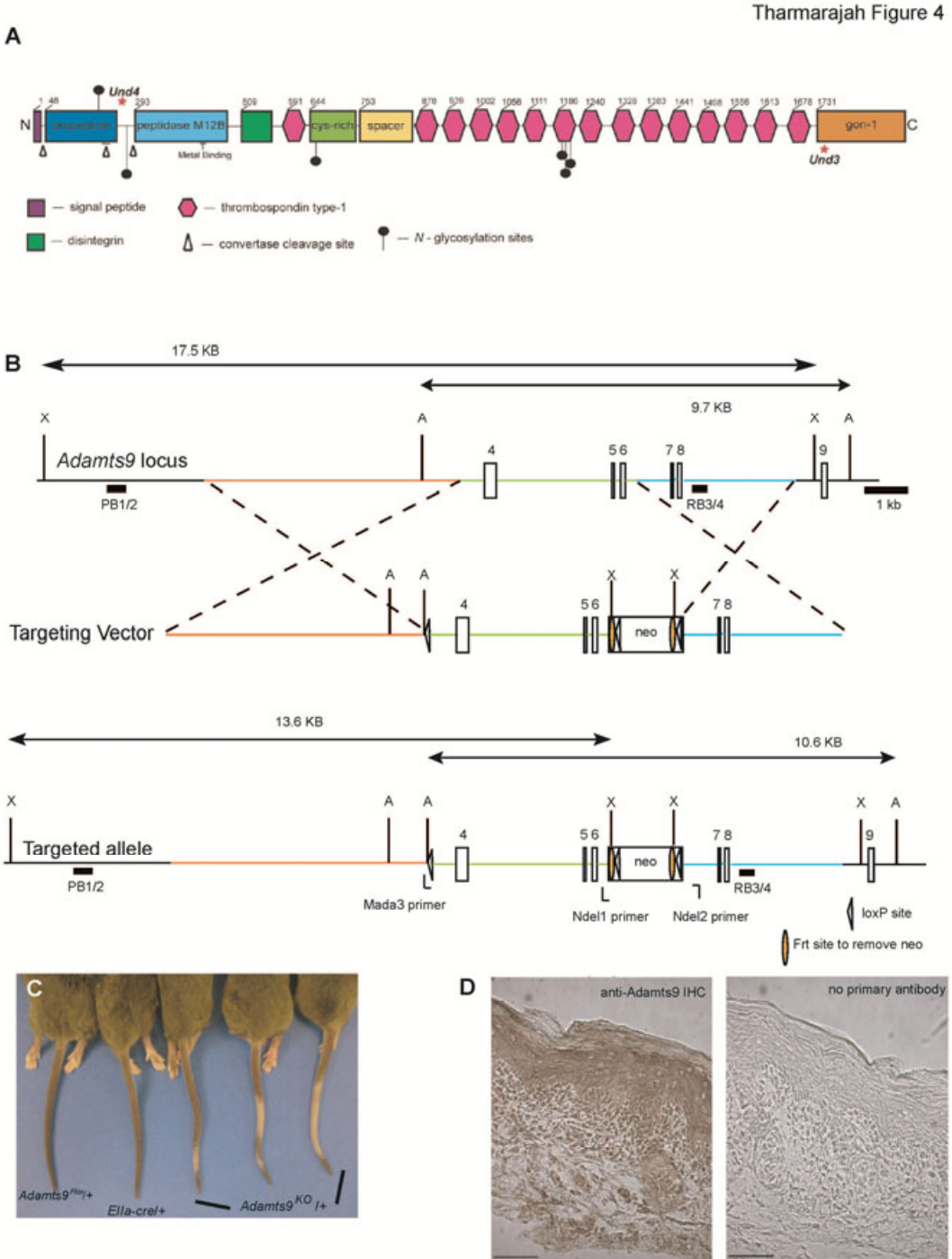

Tharmarajah Figure 5

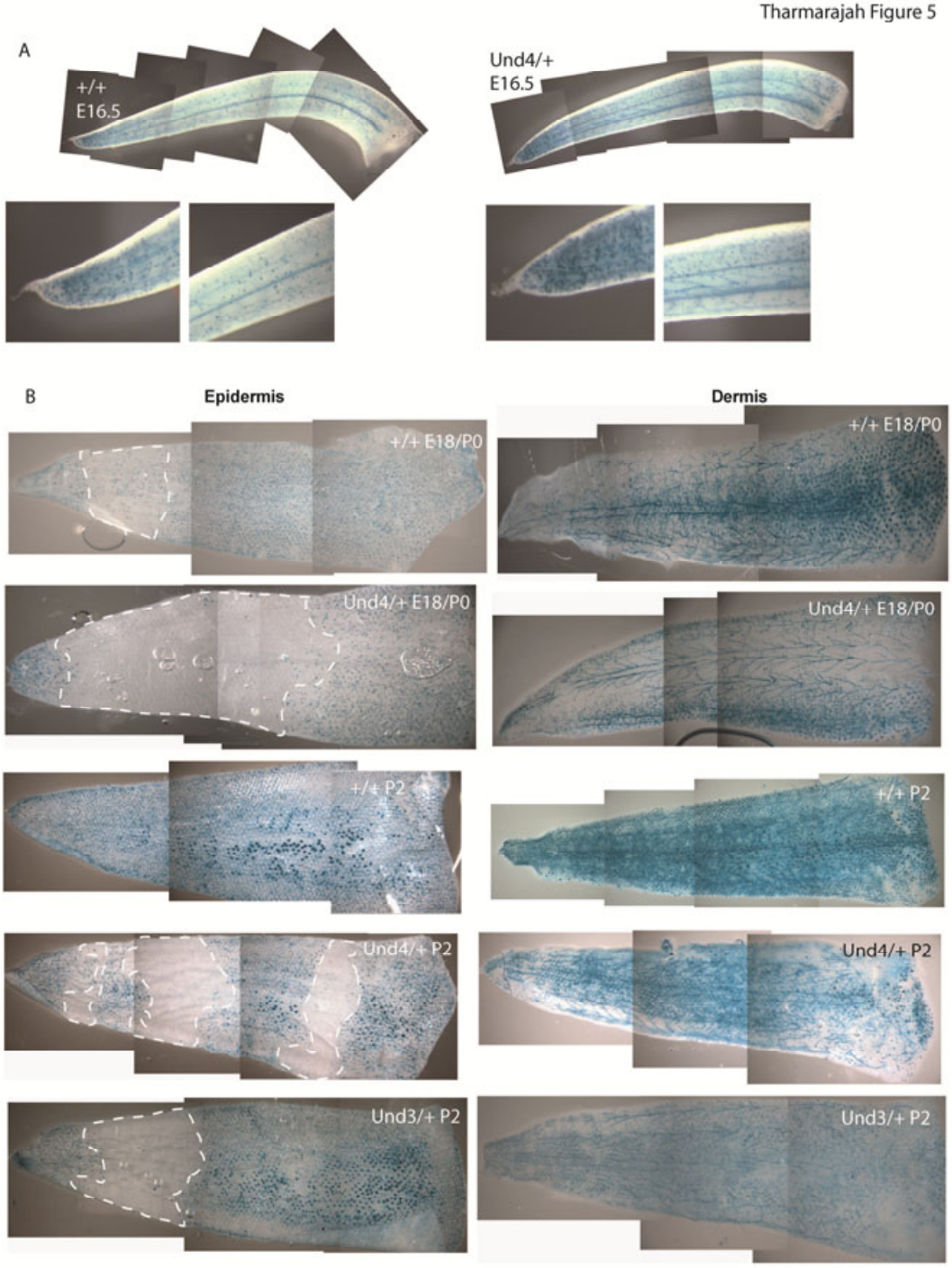

Tharmarajah et al Figure 7